ACS APPLIED MATERIALS & INTERFACES

Research Article

Cite This: ACS Appl. Mater. Interfaces 2019, 11, 16040−16047

www.acsami.org

Biobased Cellulose Nanofibril−Oil Composite Films for Active Edible Barriers

Luis Valencia,*[,†] Emma M. Nomena,[‡,§] Aji P. Mathew,[†] and Krassimir P. Velikov*[,‡,§,∥]

[†]Division of Materials and Environmental Chemistry, Stockholm University, Frescativägen 8, 10691 Stockholm, Sweden

[‡]Unilever R&D Vlaardingen, Olivier van Nortlaan 120, 3133 AT Vlaardingen, The Netherlands

[§]Institute of Physics, University of Amsterdam, Science Park 904, 1098 XH Amsterdam, The Netherlands

[∥]Soft Condensed Matter, Debye Institute for Nanomaterials Science, Utrecht University, Princetonplein 5, 3584 CC Utrecht, The Netherlands

Supporting Information

ABSTRACT: Low-concentration oil-in-water emulsions stabilized by cellulose nanofibrils (CNFs) extracted from primary plant cell wall materials are used to prepare thin biobased CNF−oil composite films by solvent casting. Flexible, transparent, and biodegradable composite films are obtained, with increased thermal stability (up to 300 °C) as the oil concentration increases. Examination of the microstructure demonstrates a clear dependency on the oil content, as a multilayered structure where the oil phase trapped between two layers of CNFs is appreciated at high oil concentrations. The embedded oil significantly influences the mechanical and wetting properties of the films, confirming their potential for use in packaging systems. Encapsulation of curcumin in the composite films leads to an increased antioxidant (up to 30% radical scavenging activity) and antimicrobial activity, inhibiting the growth of foodborne bacteria such as *Escherichia coli*. The resulting composite films show promising results in the field of active packaging for applications in the food, pharmaceutical, and cosmetic industries.

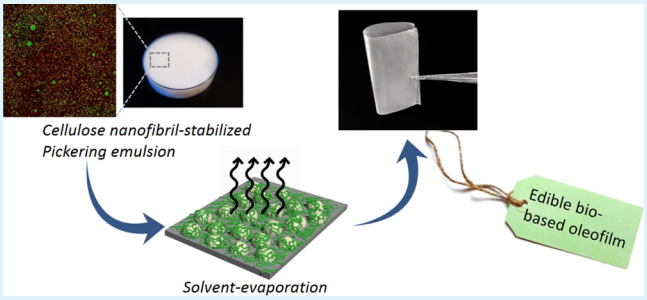

KEYWORDS: *nanocellulose, oleofilm, emulsion, active packaging, edible barrier*

INTRODUCTION

Nowadays, there is an urgent need of replacing petroleum-based polymeric materials, which represent a big environmental concern because of their nonrenewability and poor biodegradability. Current packaging materials not only consume our limited natural resources but also lead to all kind of waste, from which around 8 million metric tons of plastic wound up in the ocean every year,[1] threatening not only the surrounding environment but also human health.[2] In this sense, the development of renewable materials that follow the principles of sustainability has become a necessity.

During the last decades, extensive research effort has been destined to utilize bio-based materials from renewable resources.[3] Among them, nanocellulose (i.e., nanowhiskers, nanofibrils) extracted from different biomass sources has emerged as a key sustainable alternative because of its outstanding mechanical properties, biodegradability, low cost, and renewable nature.[4−6] Several approaches for nanocellulose-based packaging materials have been developed during the last years, nevertheless, preserving food stability and quality, without the need of further chemical modifications or additives that increment the environmental impact, remains still a challenge.[4]

Recently, some innovative works have turned their attention into Pickering emulsions as templates or intermediaries for structured materials, where biopolymers can be used as emulsifiers because of their multi-anchoring amphiphilic nature.[7,8] This has recently led to the development of low-density biopolymer-based porous materials, oleofilms, and 3D-printed scaffolds,[7,9−12] which represent an attractive alternative from an environmental point of view as they do not require additional surface-active agents. However, the preparation of cellulose nanofibrils (CNFs)-based oleofilms with potential application in food-active packaging that utilize the unique properties of CNFs has never been demonstrated.

Herein, we report for the very first time, a simple and straightforward method to obtain thin-layered translucent composite films by casting CNF-stabilized Pickering emulsions. The resulting films are fully edible and biodegradable. Microscopic characterization techniques were used to elucidate the microstructure of the films at different oil concentrations. The properties of the films for packaging solutions were assessed in terms of mechanical stiffness, thermal properties,

Received: February 12, 2019
Accepted: April 12, 2019
Published: April 12, 2019

DOI: 10.1021/acsami.9b02649
ACS Appl. Mater. Interfaces 2019, 11, 16040−16047

moisture uptake, transparency, and wettability. Moreover, we demonstrate that the oil phase that is stabilized in the dried films allows the encapsulation of lipophilic bioactive compounds, such as curcumin, opening a wide window of opportunities to tailor specific properties such as antimicrobial and antioxidant activity for active barriers.

EXPERIMENTAL PART

Materials. Soybean oil was obtained from Sigma-Aldrich (Sigma-Aldrich—S7381) and used as received (density = 0.9191 g/mL). Herbacel AQ + type N from Herbafood Ingredients GmbH Germany (84−90 wt % dietary fiber, 4−9 wt % water, 2−5 wt % ash) was used as the cellulose raw material originated from citrus peels (lot number: 30902065) and used as received. It contains around 60 wt % of cellulose, 3.4 wt % of hemicellulose, and 5 wt % of proteinaceous materials.[13] Curcumin (>94% curcuminoid content) and 2,2-diphenyl-1-picrylhydrazyl (DPPH) were purchased from Sigma-Aldrich and were used as received.

Preparation of Emulsions. The citrus fiber powder was first suspended in deionized water and thoroughly mixed using a LM5-A Silverson laboratory mixer (Silverson, USA) with a 1 mm screen hole at 3500 rpm for 5 min and afterward passed once through a high-pressure homogenizer (Microfluidizer M 110S (MF), Microfluidics Corp., USA) with a z-shape geometry (diameter 87 μm) operating at a pressure of 1200 bar. Then, soybean oil was added and the mixture was microfluidized at 1200 bar. All samples were stored in closed containers at 5 °C after preparation.

Encapsulation of Curcumin in Pickering Emulsions. Prior to mixing with CNFs, curcumin was added to soybean oil at the concentration of 1 mg/g and the mixture was vigorously mixed for approximately 20 min followed by centrifugation at 14 000g for 10 min to precipitate the undissolved curcumin. Concentration of curcumin in the oil phase was estimated by UV−vis spectroscopy (see Figure S11) as 5.5×10^{-6} wt %.

Preparation of Composite Films. Given amount of emulsion with the variable oil−CNF weight ratio was poured into plastic Petri dishes after degassing to remove any presence of bubbles and dried in a vacuum oven at 35 °C for 24 h.

Characterization. Confocal laser scanning microscopy (CLSM) was performed to visualize the microstructure of the emulsions by location of the CNFs and oil droplets. For localization of the CNF, the fresh emulsions were stained with Direct Yellow (Solophenyl Flavine 96 at 0.5 wt %) by adding a drop of the dyes to about 1 g of the emulsion. A drop of the resulting mix was then placed on a cover slip and micrographs of the emulsions were acquired using a Leica TCS-SP5 and DMI6000 inverted microscope (Leica GmbH, Germany). Fluorescence from the samples was excited at 488 nm for Direct Yellow, and emission was detected at 496−555 nm. A 63× oil-immersion objective was used to scan the images at approximately 30 μm below the cover slip. To image the oil droplets, fresh emulsions were stained by mixing around 1 g of the samples with a drop of 1 wt % Nile blue−Nile red solution. Excitation wavelengths are 488 and 633 nm and detection was at 520−602 and 661−786 nm.

The size distributions of the oil droplets were measured by dynamic light scattering (Zetasizer Nano ZS, Malvern Instruments Ltd., Worcestershire, UK), using disposable sizing cuvettes filled with 1 mL of 0.5 wt % emulsions at 25 °C. Data were collected after 2 min equilibration time and averaged over 10 measurements. The refractive indexes used for soybean oil and water were 1.47 and 1.33, respectively. The particle size was characterized by intensity-averaged mean and polydispersity index.

X-ray Photoelectron Spectroscopy. Analyses were collected with an AXIS Ultra DLD electron spectrometer (Kratos Analytical Ltd., U.K.) using a monochromatized Al Kα radiation operating at 150 W and energy of 20 eV for individual photoelectron lines. All the binding energies were referenced to the C 1s hydrocarbon peak at 284.6 eV. The high-resolution C 1s spectrum was fitted using a Shirley background subtraction and a series of Gaussian peaks, USA.

The uniaxial mechanical properties of the films were measured through a tensile test using a Zwick mechanical testing machine (model ZO10) at a crosshead speed of 5 mm/min with a gauge length of 20 mm. The measurements were carried at 50% humidity and 25 °C. The reported results were the average of calculating five specimens per sample.

The thermal behavior of the composite films was assessed by thermogravimetric analyses using a TA Instruments Discovery thermal analyzer, for measuring the mass transformation as a function of temperature, in an interval of 30−600 °C, at a heating rate of 5 °C/min. The samples were exposed to nitrogen gas at a flow rate of 20 mL/min and the nitrogen flow in the balance was 10 mL/min.

The morphology of the samples was examined by scanning electron microscopy (SEM) conducted on a JEOL 7000 with an accelerated voltage of 2 kV. The specimens were coated with a thin gold layer prior visualization.

The transparency of the films was measured using a Lambda 650 S UV−vis spectrometer, measuring in the range of 250−800 nm in the transmission mode.

The surface hydrophobicity of the films was determined by the sessile drop method using a goniometer (Drop Shape Analysis System, DSA100, Krüss GmbH, Germany). A water droplet was carefully dropped onto the films, and the drop shape was monitored for 90 s using a digital camera. The contact angle value was obtained by measuring the angle between the film surface and the tangent line at the point of contact with the water droplet.

Antioxidant Activity. The antioxidant activity of the composite films was determined by the DPPH antioxidant assay. The test consisted in adding 100 mg of the composite film into a 50 μM DPPH solution in ethanol. The reaction mixtures were kept at 30 °C in darkness and the absorbance was measured at 517 nm overtime by using an ultraviolet−visible (UV−vis) spectrophotometer. The reduction in radical scavenging activity (%-RSA) was calculated following previous reports,[14] and expressed as follows

$$\mathrm{RSA}\,(t) = 100 - \frac{A_{\mathrm{blank}(t)} - A_{\mathrm{sample}(t)}}{A_{\mathrm{blank}(t)}} \times 100 \quad (1)$$

where $A_{\mathrm{blank}(t)}$ is the absorbance measured for the DPPH solution, and $A_{\mathrm{sample}(t)}$ is the absorbance measured for the DPPH containing the film samples at the same time t.

Antimicrobial Activity. The antimicrobial activity of the films containing curcumin was assessed using the strain *Escherichia coli K12*. For the tests, exponentially growing cultures of *E. coli* were diluted to approximately 200 cells/mL. Diluted cultures were placed on the films inside of polystyrene cell culture wells and incubated without stirring for 24 h at 37 °C. The films were then carefully washed with distilled water to remove planktonic and loosely attached cells. The visualization of the bacterial cells was performed by confocal microscopy 24 h after inoculation using a Leica TCS-SP5 and DMI6000 inverted microscope (Leica GmbH, Germany). Viable and nonviable bacteria were tracked using the Live/Dead BacLight Bacterial Viability Kit (Sigma-Aldrich). For staining, the surface of each specimen was covered with 100 μL of stain (a 2:1 mixture of calcein-AM and propidium iodide in buffer solution), then incubated at 37 °C for 15 min before imaging. Calcein-AM stains viable cells only (excitation: 488 nm, emission: 500−530 nm), while propidium iodide stains dead cells (excitation: 488 nm, emission 600−630 nm). Composite films without curcumin were used as references.

RESULTS AND DISCUSSION

A conceptual schematic illustration of the preparation of CNF−oil composite films is shown in Figure 1a. First, the suspension of CNFs (0.5 wt %), prepared by mechanical defibrillation of citrus fiber, was mixed with soybean oil, followed by microfluidization which resulted in a stable emulsion (Figure 1b) with oil droplet sizes ranging from 60 to 700 nm (assessed by dynamic light scattering). The droplet size of these emulsions can be tuned and depends linearly on

DOI: 10.1021/acsami.9b02649
ACS Appl. Mater. Interfaces 2019, 11, 16040−16047

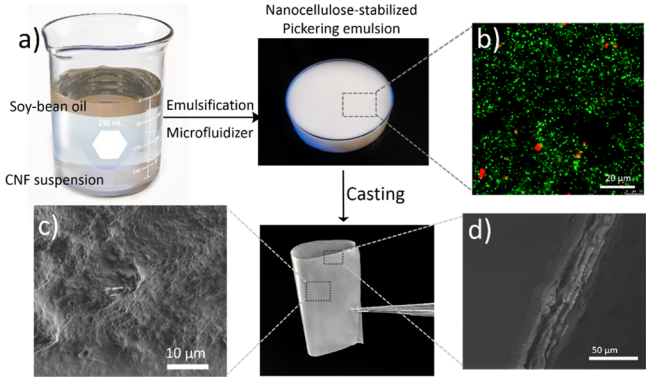

Figure 1. (a) Schematic illustration of the preparation of the CNF–oil composite films; (b) CLSM micrograph of the prepared emulsion showing the oil droplets; (c) SEM micrograph displaying the (c) surface topography; and (d) cross-sectional image of the CNF–oil composite films.

the volume fraction of oil in the emulsion (see Figures S1 and S2). Depletion effects of the nonadsorbed CNFs explain the stability of the emulsions against creaming.[15]

Microstructure of the Composite Films. The preparation of the composite films was carried out by the conventional casting method, leaving the emulsion to evaporate at room temperature in a Petri dish, which resulted in a transparent flexible thin film with minimal oil separation. The process is schematically illustrated in Figure 1.

To further understand the distribution of the oil and CNF phase, the surface topography of the films was analyzed by SEM and the results are shown in Figure 2e–h, as well as the cross-sectional microscopy images of the films (see Figure 2a–d). From the images, one can observe that the drying led to a complete coalescence of the all the oil droplets, leading to a uniform oil layer that homogeneously permeate the CNF network. Moreover, at low oil concentrations, a uniform CNF–oil composite film was observed with no oil pockets. When the concentration of oil increased, the oil was mainly observed between layers of nanofibers, forming an apparent multilayered "sandwich-like" structure, where a rigid layer of CNFs covered the surface (Figure 2a–d). This layered structure is most prevalent at the highest oil concentrations, where successive layers of oil and CNFs can be observed. The different structure formation of the composite films depending on the oil content is schematically represented in Figure 3.

The different microstructure formation of the composite films was corroborated by confocal microscopy using Direct Yellow as the staining agent to visualize the CNF, and Nile red to image the oil phase, and a mixture of them to visualize the overlay of both phases. The results, shown in Figure 4, demonstrate that at low oil content, the oil is apparently interpenetrated in the CNF network, forming a composite film that is relatively homogenous throughout the sample: no voids or holes were observed. SEM micrographs also confirmed the homogeneity and smoothness of the film surface without apparent pores or cracks (Figure 2a–d), indicating that the CNFs were uniformly dispersed on the surface of the films.

Physical Properties of Composite Films. The macroscopic properties of the films were analyzed in order to understand the influence of oil content over the potential performance of the composite films. The transparency of the films was assessed by UV–vis spectroscopy (Figure 5a), and the results show that the transparency gradually decreased

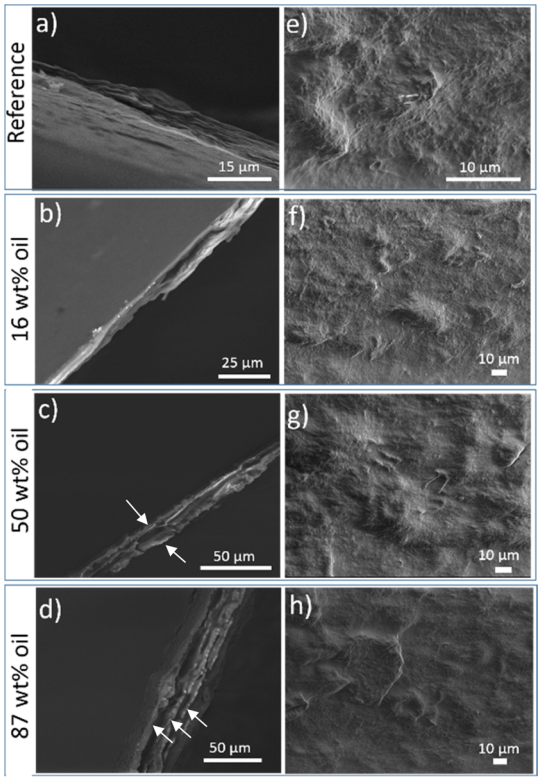

Figure 2. SEM images of the CNF–oil composite films with variable oil-content: (a–d) cross-sectional view and (e–h) top view. The amount of CNF was the same for all the samples (0.5 wt % in the aqueous phase of the emulsions). The arrows point to the layers of CNFs between which the oil layer is present.

upon incorporation of the oil. In order to understand this phenomenon, we calculated the mass attenuation coefficient, derived from the Beer–Lambert law as

$$I = I_0\, e^{-\mu x} \tag{2}$$

where I and I_0 are the original and transmitted intensities, respectively (I/I_0 is the transmission), μ is the mass attenuation coefficient of the sample (cm^2/g) while x is the mass thickness, obtained by multiplying the sample thickness with the density of the composite material, calculated by adding up the densities of the individuals weighted by respective volume fractions.

Figure 5b displays the mass attenuation coefficient of the composite films as a function of oil content. As it can be observed, a sharp nonlinear increase in the attenuation coefficient takes place upon incorporation of 16 wt % of oil into the composite films, explained by the change in composition of the films, where oil has a higher refractive index than air and water, which might be present in the hygroscopic pure CNF film. Upon further increase in oil content, the attenuation coefficient increased linearly, suggesting the dependence only in the film mass thickness and thus filler (i.e., oil) concentration in the composite films.

The composite films also exhibited an increased absorptivity at wavelengths below 300 nm (see Figure 5c): the transmittance reaches almost zero at the highest oil concentrations, which could be attributed to the UVB and UVC-blocking potential of soybean oil.[16] This property could have great implications in food-packaging applications, as UV light is known to induce auto-oxidation of fats, as well as causing

DOI: 10.1021/acsami.9b02649
ACS Appl. Mater. Interfaces 2019, 11, 16040–16047

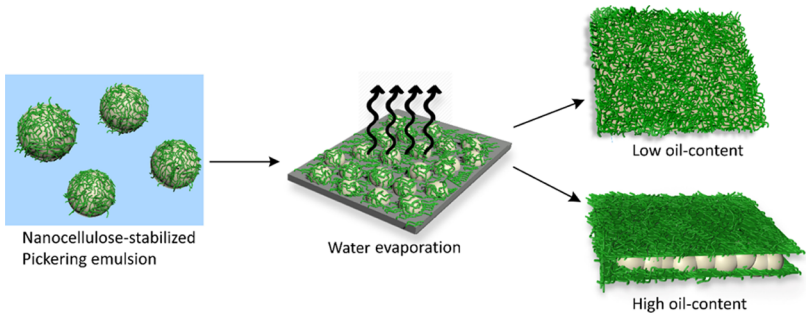

Figure 3. Schematic diagram of the formation of the CNF−oil composite films with low or high oil content.

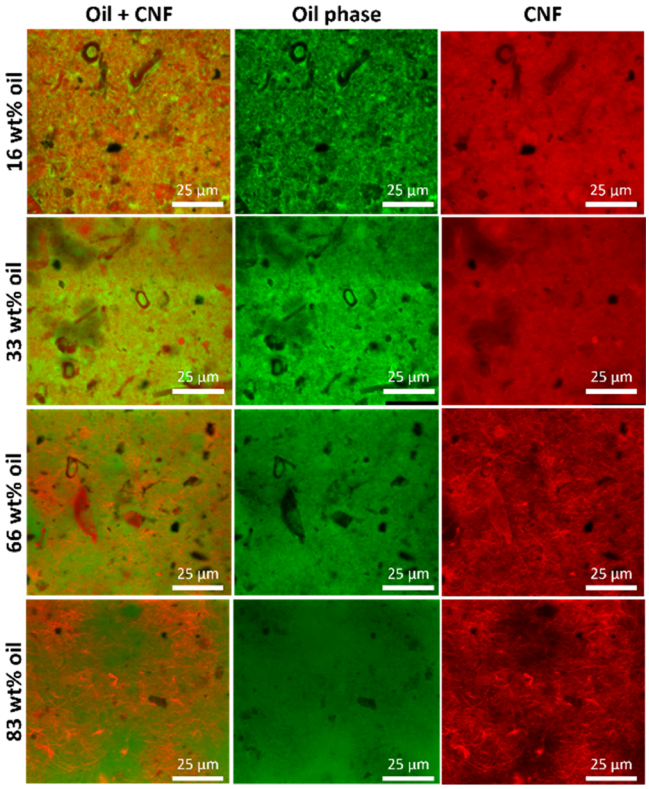

Figure 4. CLSM micrographs of the composite films showing CNFs in red, the oil phase in green, and an overlay, showing the homogenous distribution of both phases in the film.

discoloration of fresh meat, degradation of vitamins, and development of off-flavors.[17]

The surface hydrophobicity was assessed from the wettability measurement of the composite film samples, and the contact angle values as a function of time are reported in Figures 5d and S5. The films displayed a higher contact angle than the neat CNF film, proving the presence of the oil over the surface of the film, and the improved water resistance of the films, which is an essential parameter for materials destined to packaging applications. In addition, we investigated the influence of oil content over the contact-angle evolution as a function of time by means of a semiquantitative exponential decay expressed as[18,19]

$$\theta(t) = \theta_i \exp(-kt^n) \quad (3)$$

where θ_i is the initial air−water-film contact angle, right after deposition on the film surface, while k and n are the kinetic constant and the exponential parameter, respectively. The parameters for the kinetic constant and the exponential parameter determined for the composite films with different oil contents are shown in Table 1.

As shown in Table 1, the incorporation of oil induced a significant increase in the initial water contact angle (θ_i) of the films. The hydrophobicity increased from 64°, corresponding to the neat CNF film, to 90° for the sample containing 16 wt % oil. This increase in surface hydrophobicity could be attributed to the loss of free functional hydroxyl groups because of the presence of oil on the surface.[20] Moreover, the kinetic constant of the contact-angle evolution (k values in Table 1) was significantly lower for the composite film containing 16 wt % oil ($k = 6 \times 10^{-3}$ s^{-1}), compared to pure CNF ($k = 18 \times 10^{-2}$ s^{-1}), indicating a much slower adsorption/spreading process of the water droplet on the surface of the composite films.

On the other hand, a striking difference in surface hydrophobicity and the kinetic constant was observed between low and high oil concentrations (see Table 1): the films with a lower oil content are more hydrophobic than the ones with higher oil content. We assume this is due to the difference in the film microstructure (Figure 3). At low concentrations, the CNF and oil phases seem interwoven together making a composite film on the surface of which both oil and cellulose is present, while at high concentrations of oil, the layered structure is formed: successive layers of oil and CNFs. In this case, the wetting properties of the film are dominated by CNF. The exponential parameter n was also derived from the fitting approach (see eq 3 and Table 1), which, as it has been previously suggested,[18] indicates whether the contact-angle evolution arises from absorption or spreading of the water droplet on the surface of the films, assuming values between 0 (pure adsorption) and 1 (pure spreading).[19]

The mechanical properties of the films, measured from uniaxial tensile testing (Figure 5e), clearly exhibited a linear dependence on the oil content: as the oil content increased, the material became more ductile, implying that the oil acted as a plasticizer, and as the oil content increased, the film could adsorb higher amount of energy before rupture. This is an important property for an adequate design of packaging-destined films, which must have a certain degree of resistance and flexibility. While the tensile strength decreased with increasing oil concentration, the elongation at break increased dramatically especially at higher oil concentrations (see Figure 5f), leading to a very flexible film. This could be attributed to the presence of oil inclusions in the films, weakening the film cohesion and resistance. Higher oil concentrations limit the aggregation of CNFs, as observed in Figure 2a−d by the layered structure; this facilitates polymer chain displacement and allows the films to bend and stretch further without

DOI: 10.1021/acsami.9b02649
ACS Appl. Mater. Interfaces 2019, 11, 16040−16047

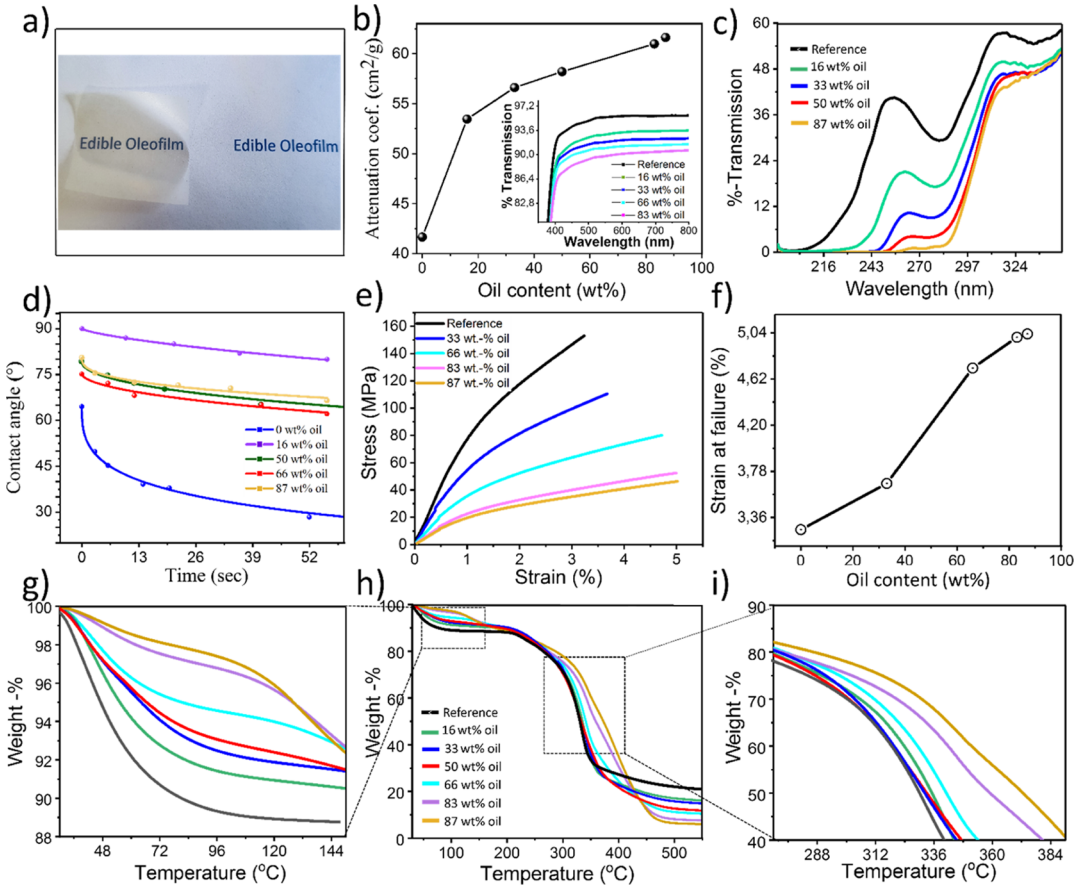

Figure 5. Physical properties of the CNF−oil composite films: (a) photograph showing the transparency of the films (87 wt % oil); (b) optical transmission of films at the visible-wavelength range and mass attenuation coefficient of composite films at λ = 700 nm; (c) optical transmission of films in the UV-spectral range; (d) experimental and fitted dynamic contact angle of composite films: the solid lines were obtained by fitting eq 3 to the experimental data (spheres); (f−e) uniaxial tensile properties of films with different oil contents; and (g−i) thermal properties of films.

Table 1. Kinetic Constant (k) and the Exponential Parameter (n) of the Contact Angle as a Function of Time for the CNF/Oil Composite Films with Different Oil Contents

Oil content (wt %)	θ_i (deg)	k (s^{-1})	n	R^2
0	64.50 ± 1.04	0.18 ± 0.017	0.36 ± 0.02	0.995
16	90.04 ± 0.37	0.006 ± 0.003	0.71 ± 0.07	0.995
50	79.20 ± 1.03	0.03 ± 0.009	0.47 ± 0.07	0.982
66	75.08 ± 1.28	0.02 ± 0.013	0.54 ± 0.14	0.969
87	79.88 ± 0.87	0.03 ± 0.011	0.38 ± 0.07	0.979

breaking.[21,22] On the other hand, the toughness of the films, defined as the amount of energy that a material can absorb prior rupture (see Figure S9), displays a detrimental trend as a function of oil content, decreasing linearly from 3.1 MJ/m^3 for the pure CNF film, to 1.5 MJ/m^3 for the composite film with 87 wt % oil content.

The thermal degradation behavior of the composite films was assessed by thermogravimetric analysis, and results are shown in Figure 5h. The presence of oil clearly enhanced the thermal stability of the films, as it increased gradually as a function of oil content, which is simply explained by the higher thermal stability of oil compared to cellulose, which positively influences the thermal behavior of the composite films. Moreover, from the thermogravimetric analysis, we can also estimate the moisture uptake of the composite films, which is an essential parameter in food-active packaging applications, as adsorbed water promoted bacterial growth. For the calculation, the attention was centered in the percentage of weight loss at 100 °C (see Figure 5i), before any structural degradation of cellulose happens, and therefore assuming only mass loss because of water evaporation. The moisture uptake decreased significantly by increasing the amount of oil in the films: for the neat CNF film, a weight of 12% was observed at 100 °C, compared to 2% for the composite film containing 87 wt % oil.

The redispersibility and degradability of the composite films was tested by resubmerging them in water (see Figure 6), and interestingly, after only 2 min of submitting the films in a sonication bath, they were completely redispersed into a stable emulsion (see Figure S9). Such behavior could be attributed to the presence of oil acting as the plasticizer, getting in between the nanofibers and therefore allowing ease of redispersion. This redispersibility furthermore corroborates the edibility of the films, as they should disintegrate into oil droplets and CNFs once ingested (the triglyceride oil will be digested under action of lipases, and even in the presence of nanocellulose can delay the rate of hydrolysis,[23,24] while the cellulose part will remain intact and stay dispersed as insoluble dietary fiber[25]), besides also proving their high degree of environmental friendliness, as the rapid degradation could allow the easy recovery of the building blocks without any waste generation, for their reusability in further applications.

DOI: 10.1021/acsami.9b02649
ACS Appl. Mater. Interfaces 2019, 11, 16040−16047

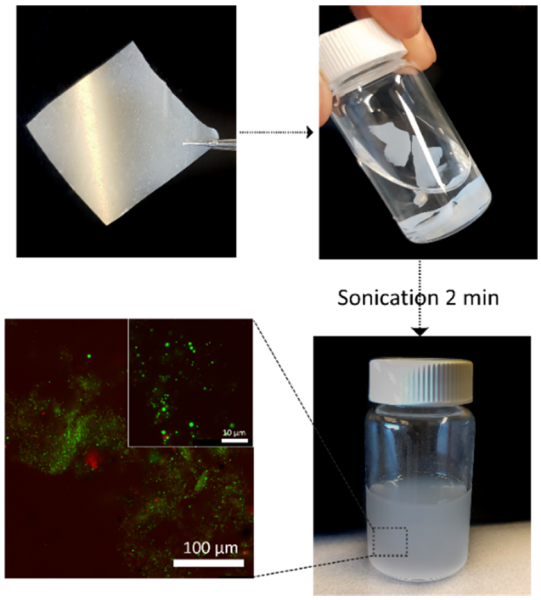

Figure 6. Schematic illustration demonstrating the biodegradability of the composite films in water in which the emulsion structure is reformed upon 2 min of sonication.

Curcumin Encapsulation in the Composite Films. Encapsulation of bioactive compounds using emulsions is a common formulation approach used in food, cosmetic, and pharmaceutical industries for incorporating high-concentrations of a substance, which can introduce specific properties or to be released over a certain time span. By using Pickering emulsions containing oil-soluble functional ingredients, we can further tune the properties of the composite films. In this work, we selected curcumin (diferuoyl methane), which is a major component of *Curcuma longa*, also known as turmeric, as a model system to be incorporated in the films. Curcumin is a phenolic nutraceutical compound which has been reported to possess therapeutic properties and to be an efficient antioxidant and reactive radical scavenger, owing to H-atom donation from the phenolic groups.[26] Curcumin have also shown to possess in vitro antimicrobial potential against a wide range of microorganisms including fungi,[27] as well as several Gram-positive and Gram-negative bacteria.[28] There are several proposed mechanisms for the antimicrobial activity of curcumin, being presumably the insertion into liposome bilayers (because of its lipophilicity and amphipathicity), enhancing the permeability of the cell membrane and eventually the rupture of intracellular components,[29,30] the most accepted one. The encapsulation of curcumin in the composite films was carried out by dissolving curcumin in the soybean oil prior to the preparation of the emulsions, followed by casting to obtain curcumin-containing films. The homogenous distribution of curcumin throughout the films could be visualized from the complete yellow tonality that the films acquired upon encapsulation (see Figure S14).

Antioxidant activity of curcumin-containing composite films. The susceptibility of food to oxidation is a major concern for the food industry, as the lipid oxidation has negative effects such as taste, appearance, texture, and shelf life, leading to the formation of off-flavors (rancidity) and toxic compounds. For this reason, introducing antioxidant properties is of paramount importance when developing active food packaging.

The antioxidant properties of the curcumin-containing composite films was assessed using the method based on the scavenging of the DPPH radical molecule, and results are shown in Figure 7a–c, where the antioxidant activity was

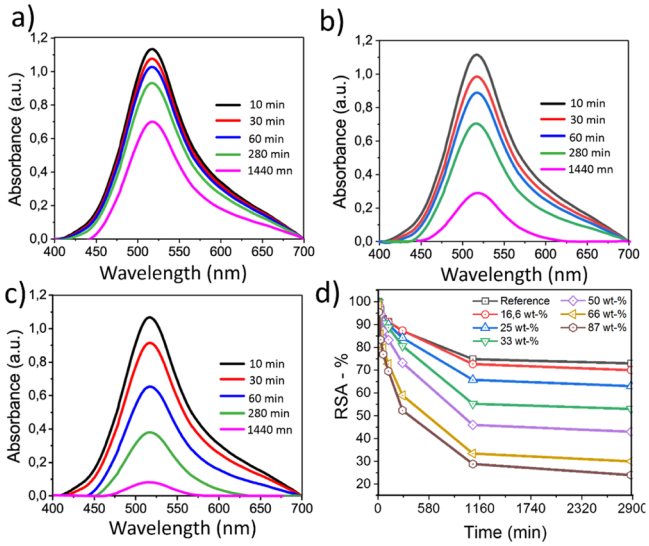

Figure 7. %-RSA of curcumin-loaded films evaluated by the DPPH method. (a–c) UV–vis spectra (baseline corrected) of DPPH + films: (a) reference, (b) film with 50 wt % oil content, and (c) film with 86 wt % oil content. (d) Reduction in scavenging activity as a function of oil content in films loaded with curcumin.

calculated by following the decrease in the absorbance band at 517 nm (see Figure 7c,d), which is the maximum absorbance band of DPPH ethanolic solution. The results in %-RSA as a function of time are shown in Figure 7d. All RSA kinetics exhibited a gradual decrease at first, followed by a slowing down of the %-RSA, to finally reach a plateau after 48 h. Moreover, clearly the %-RSA increased as a function of oil (which contains curcumin). The neat CNF film did not show any significant antioxidant activity, as expected.

Antimicrobial Activity of Curcumin-Containing Composite Films. Curcumin is known for its antibacterial and antifungal properties,[31] which makes it an ideal candidate for pathogen growth inhibition in active packaging. Its poor solubility in water is an obstacle to its use in packaging systems as an antimicrobial agent, hence the need of encapsulation to increase its delivery. The antimicrobial properties of curcumin depend on several factors such as the delivery mechanism, blue-light exposure, or type of bacteria.[32,33]

While curcumin is less effective against Gram-negative bacteria such as *E. coli*, it can nonetheless inhibit the growth of other bacteria strains depending on the mode of delivery.[34] The effect of curcumin on the antimicrobial properties of the films was assessed against *E. coli*, a common foodborne pathogen, and the results indicate that while live bacteria can still be found, bacteria growth and viability was largely inhibited compared to the samples without curcumin (Figure 8). Surprisingly, almost total bacterial impairment was observed after 24 h of incubation using low oil concentration (16 wt %), while more live bacteria subsided as the oil concentration increased. This is consistent with the increased hydrophobicity of the surface of the films, as at low oil concentrations, the microstructure of the film contains more oil at the surface (see Figure 3), hence more curcumin and a

DOI: 10.1021/acsami.9b02649
ACS Appl. Mater. Interfaces 2019, 11, 16040–16047

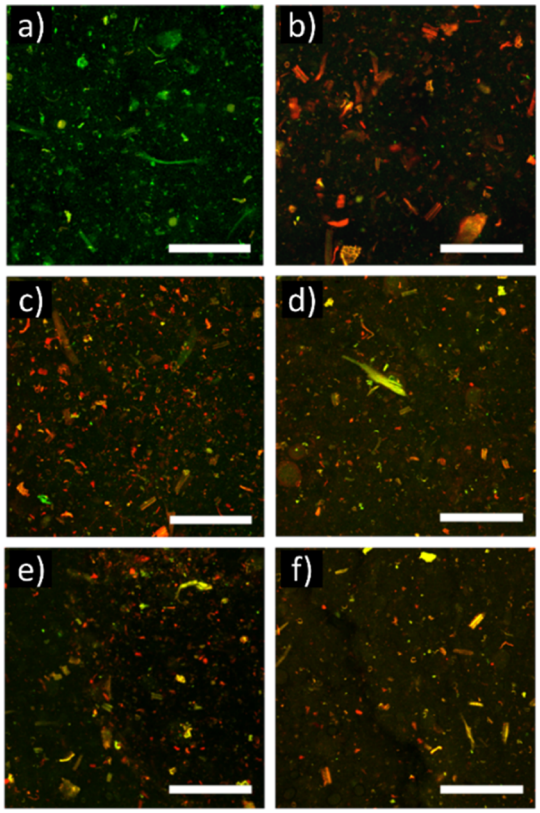

Figure 8. CSLM overlay images of showing the viability of *E. coli* 24 h after inoculation. Live cells are in green and dead ones in red. Composite film without curcumin (a) was used as the reference sample. Composite films with curcumin (5.5×10^{-6} wt % in the oil) with different oil concentrations: 16 (b), 25 (c), 50 (d), 66 (e), and 83 and 87 wt % (f). Scale bar: 250 μm.

stronger bactericidal effect. At high concentrations, the oil is located mainly between the layers of CNF, so their surface is more vulnerable to bacteria. Nevertheless, bacteria viability decreased at all oil concentrations compared to the samples without oil, indicating a possible use of the films for food-packaging applications.

CONCLUSIONS

We have demonstrated the fabrication of bio-based composite films by solvent-casting an oil-in-water emulsion stabilized by CNFs derived from plant cell wall materials. The microstructure of such films is dependent on the oil concentration: an interpenetrated network of CNF and oil is obtained at low fibril concentrations, while a layered structure of successive CNF and oil is obtained at high fibril concentrations. The optical, mechanical, and thermal properties of the films are also controlled by the oil concentration: higher oil concentrations have increased ductility and thermal stability, albeit they are less translucent. Moreover, we have shown that it is possible to encapsulate bioactive compounds in the oil phase for added functionality. Encapsulation of curcumin gives the films a higher antioxidant activity and antimicrobial properties. These features open the way to new active materials with tailored properties for use as packaging materials, drug delivery, or strategies where oxidative degradation and microbial growth need to be inhibited.

ASSOCIATED CONTENT

Supporting Information

The Supporting Information is available free of charge on the ACS Publications website at DOI: 10.1021/acsami.9b02649.

Photographs of the CNF-stabilized Pickering emulsions with different oil concentrations; CLSM micrographs of the emulsions with different oil concentrations; density and thickness of composite films as a function of oil content; contact angle measurements of composite films with different oil contents; C 1s and O 1s high-resolution X-ray photoelectron spectroscopy spectra of different composite films with different oil contents; transparency of the composite films with different oil contents; dynamic light scattering measurement of emulsion (0.016 wt % oil−0.05 wt % CNF) before casting and after casting and redispersion of the film; photographs and UV−vis spectra of the composite film loaded with curcumin (PDF)

AUTHOR INFORMATION

Corresponding Authors

*E-mail: luis.alexandro@mmk.su.se (L.V.).
*E-mail: krassimir.velikov@unilever.com (K.V.).

ORCID

Luis Valencia: 0000-0001-6572-7460
Emma M. Nomena: 0000-0003-0304-9865
Aji P. Mathew: 0000-0001-8909-3554
Krassimir P. Velikov: 0000-0002-8838-1201

Author Contributions

L.V. and E.M.N. contributed equally to this work. The manuscript was written through contributions of all the authors. All the authors have given approval to the final version of the manuscript.

Notes

The authors declare no competing financial interest.

ACKNOWLEDGMENTS

This project has received funding from the European Union's Horizon 2020 research and innovation program under grant agreement nos 674979-NANOTRANS and 676045-MULTIMAT. We thank Dr Luben Arnaudov for his assistance with contact-angle measurements and Rinus van Triet and Robert Hoeve for their help with the tensile tests and transparency measurements. We also thank Dr Jan-Willem Sanders and Leonie van Schie for providing the *E. coli* strain and helping with inoculation.

REFERENCES

(1) Jambeck, J. R.; Geyer, R.; Wilcox, C.; Siegler, T. R.; Perryman, M.; Andrady, A.; Narayan, R.; Law, K. L. Plastic Waste Inputs from Land into the Ocean. *Science* **2015**, *347*, 768−771.
(2) Kirwan, M. J.; Plant, S.; Strawbridge, J. W. Plastics in Food Packaging. *Food and Beverage Packaging Technology*; Wiley-Blackwell: Oxford, UK, 2011; pp 157−212.
(3) Wróblewska-Krepsztul, J.; Rydzkowski, T.; Borowski, G.; Szczypiński, M.; Klepka, T.; Thakur, V. K. Recent Progress in Biodegradable Polymers and Nanocomposite-Based Packaging Materials for Sustainable Environment. *Int. J. Polym. Anal. Charact.* **2018**, *23*, 383−395.
(4) Ferrer, A.; Pal, L.; Hubbe, M. Nanocellulose in Packaging: Advances in Barrier Layer Technologies. *Ind. Crops Prod.* **2017**, *95*, 574−582.

DOI: 10.1021/acsami.9b02649
ACS Appl. Mater. Interfaces 2019, 11, 16040−16047

(5) Thomas, B.; Raj, M. C.; Athira, K. B.; Rubiyah, M. H.; Joy, J.; Moores, A.; Drisko, G. L.; Sanchez, C. Nanocellulose, a Versatile Green Platform: From Biosources to Materials and Their Applications. *Chem. Rev.* **2018**, *118*, 11575−11625.
(6) Valencia, L.; Arumughan, V.; Jalvo, B.; Maria, H. J.; Thomas, S.; Mathew, A. P. Nanolignocellulose Extracted from Environmentally Undesired *Prosopis Juliflora*. *ACS Omega* **2019**, *4*, 4330−4338.
(7) Jiménez-Saelices, C.; Seantier, B.; Grohens, Y.; Capron, I. Thermal Superinsulating Materials Made from Nanofibrillated Cellulose-Stabilized Pickering Emulsions. *ACS Appl. Mater. Interfaces* **2018**, *10*, 16193−16202.
(8) Patel, A. R. Functional and Engineered Colloids from Edible Materials for Emerging Applications in Designing the Food of the Future. *Adv. Funct. Mater.* **2018**, 1806809.
(9) Tasset, S.; Cathala, B.; Bizot, H.; Capron, I. Versatile Cellular Foams Derived from CNC-Stabilized Pickering Emulsions. *RSC Adv.* **2014**, *4*, 893−898.
(10) Wijaya, W.; Van der Meeren, P.; Dewettinck, K.; Patel, A. R. High Internal Phase Emulsion (HIPE)-Templated Biopolymeric Oleofilms Containing an Ultra-High Concentration of Edible Liquid Oil. *Food Funct.* **2018**, *9*, 1993−1997.
(11) Kim, K.; Kim, S.; Ryu, J.; Jeon, J.; Jang, S. G.; Kim, H.; Gweon, D.-G.; Im, W. B.; Han, Y.; Kim, H.; et al. Processable High Internal Phase Pickering Emulsions Using Depletion Attraction. *Nat. Commun.* **2017**, *8*, 14305.
(12) Yang, T.; Hu, Y.; Wang, C.; Binks, B. P. Fabrication of Hierarchical Macroporous Biocompatible Scaffolds by Combining Pickering High Internal Phase Emulsion Templates with Three-Dimensional Printing. *ACS Appl. Mater. Interfaces* **2017**, *9*, 22950−22958.
(13) Fechner, A.; Fenske, K.; Jahreis, G. Effects of Legume Kernel Fibres and Citrus Fibre on Putative Risk Factors for Colorectal Cancer: A Randomised, Double-Blind, Crossover Human Intervention Trial. *Nutr. J.* **2013**, *12*, 101.
(14) Crouvisier-Urion, K.; Bodart, P. R.; Winckler, P.; Raya, J.; Gougeon, R. D.; Cayot, P.; Domenek, S.; Debeaufort, F.; Karbowiak, T. Biobased Composite Films from Chitosan and Lignin: Antioxidant Activity Related to Structure and Moisture. *ACS Sustainable Chem. Eng.* **2016**, *4*, 6371−6381.
(15) Nomena, E. M.; Remijn, C.; Rogier, F.; van der Vaart, M.; Voudouris, P.; Velikov, K. P. Unravelling the Mechanism of Stabilization and Microstructure of Oil-in-Water Emulsions by Native Cellulose Microfibrils in Primary Plant Cells Dispersions. *ACS Appl. Bio Mater.* **2018**, *1*, 1440−1447.
(16) Bonina, F.; Puglia, C.; Avogadro, M.; Baranelli, E.; Cravotto, G. The Topical Protective Effect of Soybean-Germ Oil against UVB-Induced Cutaneous Erythema: Anin Vivo Evaluation. *Arch. Pharm.* **2005**, *338*, 598−601.
(17) Thron, M.; Eichner, K.; Ziegleder, G. The Influence of Light of Different Wavelengths on Chlorophyll-Containing Foods. *Food Sci. Technol.* **2001**, *34*, 542−548.
(18) Farris, S.; Introzzi, L.; Biagioni, P.; Holz, T.; Schiraldi, A.; Piergiovanni, L. Wetting of biopolymer coatings: contact angle kinetics and image analysis investigation. *Langmuir* **2011**, *27*, 7563−7574.
(19) Bertolino, V.; Cavallaro, G.; Lazzara, G.; Milioto, S.; Parisi, F. Halloysite Nanotubes Sandwiched between Chitosan Layers: Novel Bionanocomposites with Multilayer Structures. *New J. Chem.* **2018**, *42*, 8384−8390.
(20) Ojagh, S. M.; Rezaei, M.; Razavi, S. H.; Hosseini, S. M. H. Development and Evaluation of a Novel Biodegradable Film Made from Chitosan and Cinnamon Essential Oil with Low Affinity toward Water. *Food Chem.* **2010**, *122*, 161−166.
(21) Ahmad, M.; Benjakul, S.; Prodpran, T.; Agustini, T. W. Physico-Mechanical and Antimicrobial Properties of Gelatin Film from the Skin of Unicorn Leatherjacket Incorporated with Essential Oils. *Food Hydrocolloids* **2012**, *28*, 189−199.
(22) Bonilla, J.; Atarés, L.; Vargas, M.; Chiralt, A. Effect of Essential Oils and Homogenization Conditions on Properties of Chitosan-Based Films. *Food Hydrocolloids* **2012**, *26*, 9−16.
(23) DeLoid, G. M.; Sohal, I. S.; Lorente, L. R.; Molina, R. M.; Pyrgiotakis, G.; Stevanovic, A.; Zhang, R.; McClements, D. J.; Geitner, N. K.; Bousfield, D. W.; et al. Reducing Intestinal Digestion and Absorption of Fat Using a Nature-Derived Biopolymer: Interference of Triglyceride Hydrolysis by Nanocellulose. *ACS Nano* **2018**, *12*, 6469−6479.
(24) Liu, L.; Kerr, W. L.; Kong, F. Characterization of lipid emulsions during in vitro digestion in the presence of three types of nanocellulose. *J. Colloid Interface Sci.* **2019**, *545*, 317−329.
(25) Dhingra, D.; Michael, M.; Rajput, H.; Patil, R. T. Dietary Fibre in Foods: A Review. *J. Food Sci. Technol.* **2012**, *49*, 255−266.
(26) Ak, T.; Gülçin, İ. Antioxidant and Radical Scavenging Properties of Curcumin. *Chem.-Biol. Interact.* **2008**, *174*, 27−37.
(27) Neelofar, K.; Shreaz, S.; Rimple, B.; Muralidhar, S.; Nikhat, M.; Khan, L. A. Curcumin as a Promising Anticandidal of Clinical Interest. *Can. J. Microbiol.* **2011**, *57*, 204−210.
(28) Mun, S.-H.; Joung, D.-K.; Kim, Y.-S.; Kang, O.-H.; Kim, S.-B.; Seo, Y.-S.; Kim, Y.-C.; Lee, D.-S.; Shin, D.-W.; Kweon, K.-T.; et al. Synergistic Antibacterial Effect of Curcumin against Methicillin-Resistant Staphylococcus Aureus. *Phytomedicine* **2013**, *20*, 714−718.
(29) Varshney, G. K.; Saini, R. K.; Gupta, P. K.; Das, K. Effect of Curcumin on the Diffusion Kinetics of a Hemicyanine Dye, LDS-698, across a Lipid Bilayer Probed by Second Harmonic Spectroscopy. *Langmuir* **2013**, *29*, 2912−2918.
(30) Tyagi, P.; Singh, M.; Kumari, H.; Kumari, A.; Mukhopadhyay, K. Bactericidal Activity of Curcumin I Is Associated with Damaging of Bacterial Membrane. *PLoS One* **2015**, *10*, No. e0121313.
(31) Moghadamtousi, S. Z.; Kadir, H. A.; Hassandarvish, P.; Tajik, H.; Abubakar, S.; Zandi, K. A review on antibacterial, antiviral, and antifungal activity of curcumin. *Biomed Res. Int.* **2014**, *2014*, 186864.
(32) Yallapu, M. M.; Nagesh, P. K. B.; Jaggi, M.; Chauhan, S. C. Therapeutic Applications of Curcumin Nanoformulations. *AAPS J.* **2015**, *17*, 1341−1356.
(33) Hegge, A. B.; Bruzell, E.; Kristensen, S.; Tønnesen, H. H. Photoinactivation of Staphylococcus epidermidis biofilms and suspensions by the hydrophobic photosensitizer curcumin - Effect of selected nanocarrier. *Eur. J. Pharm. Sci.* **2012**, *47*, 65−74.
(34) Shlar, I.; Droby, S.; Choudhary, R.; Rodov, V. The Mode of Antimicrobial Action of Curcumin Depends on the Delivery System: Monolithic Nanoparticles vs. Supramolecular Inclusion Complex. *RSC Adv.* **2017**, *7*, 42559−42569.

DOI: 10.1021/acsami.9b02649
ACS Appl. Mater. Interfaces 2019, 11, 16040−16047